International Journal of Applied Earth Observation and Geoinformation 52 (2016) 1–11

Contents lists available at ScienceDirect

International Journal of Applied Earth Observation and Geoinformation

journal homepage: www.elsevier.com/locate/jag

A new technique for the detection of large scale landslides in glacio-lacustrine deposits using image correlation based upon aerial imagery: A case study from the French Alps

Paz Fernandez [a,*], Malcolm Whitworth [b]

[a] Department of Civil Engineering, ETSICCP, University of Granada, Campus de Fuentenueva, E-18071, Granada, Spain
[b] School of Earth and Environmental Sciences, University of Portsmouth, Burnaby Road, Portsmouth PO1 3QL, United Kingdom

ARTICLE INFO

Article history:
Received 1 December 2015
Received in revised form 21 April 2016
Accepted 11 May 2016
Available online 2 June 2016

Keywords:
Image correlation
Normalised cross-correlation
Aerial photographs
Landslides
Surface deformation
Displacement measurement
Landslide monitoring.

ABSTRACT

Landslide monitoring has benefited from recent advances in the use of image correlation of high resolution optical imagery. However, this approach has typically involved satellite imagery that may not be available for all landslides depending on their time of movement and location. This study has investigated the application of image correlation techniques applied to a sequence of aerial imagery to an active landslide in the French Alps. We apply an indirect landslide monitoring technique (COSI-Corr) based upon the cross-correlation between aerial photographs, to obtain horizontal displacement rates. Results for the 2001–2003 time interval are presented, providing a spatial model of landslide activity and motion across the landslide, which is consistent with previous studies. The study has identified areas of new landslide activity in addition to known areas and through image decorrelation has identified and mapped two new lateral landslides within the main landslide complex. This new approach for landslide monitoring is likely to be of wide applicability to other areas characterised by complex ground displacements.

1. Introduction

Landslide monitoring is a very important part of any landslide hazard assessment, providing a measure of the rate and direction of slope movement in order to quantify any potential landslide risk. Different types of monitoring techniques can be employed, depending on the scale and frequency of observations required; they include in-situ instrumentation, but these provide movement data at a single location on the landslide; and are often difficult to install on very active landslides. Other options include remote ground based monitoring such as ground based radar (Monserrat et al., 2014), terrestrial laser scanning (Jaboyedoff et al., 2012; Delacourt et al., 2007; Teza et al., 2008) and multi-temporal terrestrial photography (Gance et al., 2014; Travelletti et al., 2012), but these require a clear line of sight in order to monitor the entire landslide effectively. By contrast, satellite and airborne remote sensing platforms offer better visibility and coverage of the ground surface by virtue of the vertical imaging geometry. Monitoring has been performed using digital photogrammetry applied to aerial imagery (Casson et al., 2003; Fabris et al., 2011), radar interferometry (Wasowski and Bovenga, 2014) and comparison of LiDAR derived elevation models (Daehne and Corsini, 2013). More recently, image matching has been applied to aerial and satellite imagery to monitor slope movement, by comparing two remote sensing images of a landslide from different dates to identify and quantify surface changes. This type of image matching or image correlation approach has been applied to landslide monitoring using aerial stereo-pairs and satellite imagery in this area, like aerial stereo-pairs used in La Clapiere landslide to understand its dynamics (Booth et al., 2013; Casson et al., 2003; Delacourt et al., 2007) and LiDAR point cloud data (Travelletti et al., 2012). However, there are no examples that use aerial photography and image matching as the basis for landslide monitoring. There may be occasions when satellite imagery or high resolution topographic data are unavailable, either due to the age of the movement or simply through a lack of data coverage. In these circumstances, the use of aerial photography can offer opportunities for landslide monitoring, whereby aerial imagery from two different dates can provide the basis for identifying and measuring landslide movement.

In this study, we present the application of an image matching technique to the study of an active glacio-lacustrine landslide in the French Alps, using *aerial photography* as a basis for the image correlation. This contrasts with previous studies that have princi-

* Corresponding author.
E-mail addresses: pazferol@ugr.es (P. Fernandez), malcolm.whitworth@port.ac.uk (M. Whitworth).

http://dx.doi.org/10.1016/j.jag.2016.05.002
0303-2434/

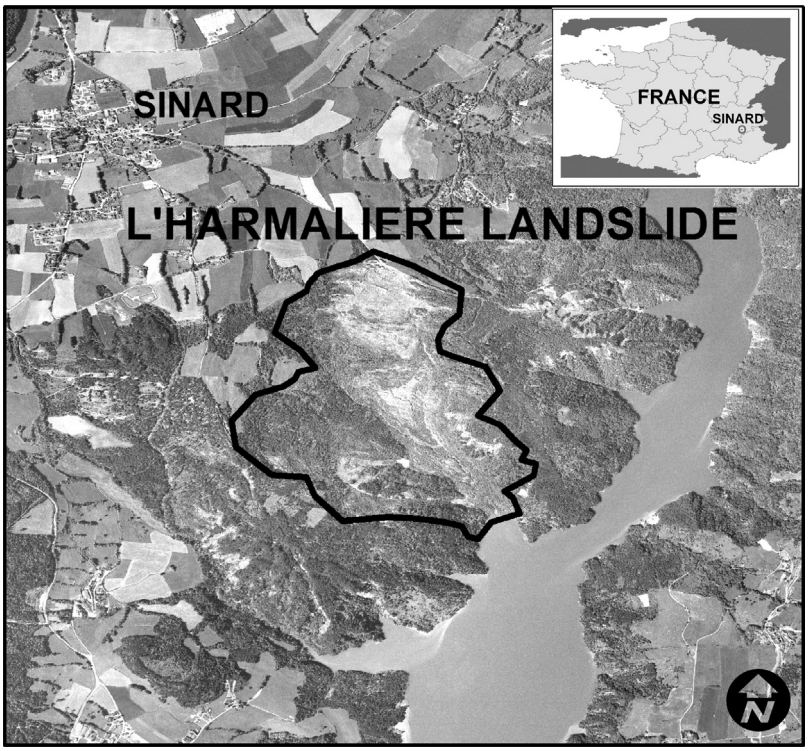

Fig. 1. Location and view of the Harmaliere landslide area with its outlines. It is situated near the village of Sinard, within the Drac valley 40 km south of the Grenoble city, France.

pally relied upon satellite platforms to provide the imagery for the comparison. We demonstrate the suitability of COSI-Corr software (Ayoub et al., 2009), to the study of landslide movement based upon aerial photography, rather than satellite imagery or topographic data; and identify the steps, information and conditions necessary for successful application to landslide monitoring. The technique has been applied in the Harmaliere landslide to firstly, identify areas of landslide activity and secondly, obtain horizontal displacement rates on the active part of the landslide.

1.1. Geological context and landslide study area

In France, some of the largest and most problematic landslides in the Alps are associated with Quaternary glacio-lacustrine deposits that infill many of the alpine valleys. These lake deposits typically consist of fine grained finely laminated (varved) silts and clays deposited in dammed lakes impounded by valley glaciers during previous glacial advances. The deposits have been exposed by the local river network that has cut down deeply into these clay formations; consequently, in many places, these deposits make up much of the slope forming materials within the valleys. The geotechnical nature of these deposits is such that this exposure has resulted in significant slope instability (Giraud et al., 1991; Van Asch et al., 2009).

The Harmaliere landslide, documented in this study, is located in the Trieves region of the French Alps, near the village of Sinard in the Drac valley, 40 km south of Grenoble in an area of extensive glacio-lacustrine deposit exposure (Fig. 1). Here the glacio-lacustrine deposits cover an area of 300 km^2 and were deposited in lakes impounded by the Isiere Glacier during the Wurm maximum episode (Van Asch et al., 2009). The thickness of the laminated clays in this region varies from 0 to 250 m, reflecting the uneven nature of the base of the lakes in which deposition took place. The deposits have been exposed by the local river network that has cut down deeply into these clay formations; consequently, in many places, including the Drac valley, these deposits make up much of the slope forming materials within the valleys. The geotechnical nature of these deposits is such that this exposure has resulted in significant slope instability, which poses a hazard to local population centres and infrastructure (Antoine, 1992; Giraud et al., 1991; Van Asch et al., 2009).

The Harmaliere landslide underwent a major initial movement in March 1981 following a period of quiescence. The main initiation event is illustrated in Figs. 2 and 3, the landslide is shown in its pre-failure state on aerial imagery acquired in 1948 (Fig. 2), this contrasts with the second image taken in 1981 (Fig. 3), just after the main activation, where the landslide can be seen to have undergone a major retrocession and advanced down the valley into the Lac de Monteynard (this lake was filled following completion of the Monteynard Dam in 1961 and so not visible in the earlier 1948 images). Since 1981 the landslide has retrogressed repeatedly through a number of episodic events at the head of the landslide in 1988, 1996 and 2001 (Bievre et al., 2011). In between, however the landslide has displayed evidence of mass redistribution throughout the slope and a number of lateral landslide events. Geotechnical investigations of the neighbouring Avignonet landslide indicates that the landslide movement in this area typically involves several slip surfaces at shallow depths of 5–15 m and depths of greater than 50 m (Jongmans et al., 2009). Consequently, a range of slide velocities are observed, as landslides of different depths respond to climatic events, such as rain and snow melt. Bievre et al. (2011) documented velocity variations between a few centimeters to several tens of metres per year across the Avignonet and Hermaliare slides, with a mean regression rate up to 10 m/year measured from aerial photographic analysis (Jongmans et al., 2009, 2008). Importantly, relict landslides are likely to be present in this area; given the length of time river erosion has been acting along the Drac valleys following glacial retreat, the river erosion and downcutting during this period of associated climatic amelioration would have resulted in a long period of landslide activity. Therefore, relict landslides are

Fig. 2. Ortho-rectified aerial image of the Hermaliere landslide site prior to failure, the *ortho*-image was generated using aerial photography taken in 1948.

postulated to exist in many of the slopes in this area, indeed the image take in 1948 (Fig. 2) provides geomorphological evidence of superficial landslide activity even prior to the major event in 1981 (Fig. 3).

Geologically, the area is characterised by an undulating carbonate bedrock that is overlain by a 250 m stack of Quaternary glacial, fluvial and lacustrine deposits formed at the frontal margin of a valley glacier (Isere Glacier). The superficial deposits are the result of a series of glacial and inter-glacial events that have affected the Alps over the past 200k years, including Wiss glaciation (200–130ky BP), Wiss-Wurm interglacial (130–100ky BP) and the most recently, the Wurm (100–12ky BP). At the peak of this latest glacial period (24–18ky BP) the region was affected by the Isere Glacier, which moved from the north, past Grenoble and into the Drac valley, subsequently terminating close to the village of Sinard nearby the Hermaliere landslide locality. The base of the Quaternary sediment sequence comprises coarse fluvio-glacial deposits that rest unconformably on the Jurassic carbonate bedrock. They

Fig. 3. Ortho-rectified aerial image of the Hermaliere landslide site showing the results of the major movement in March 1981. The *ortho*-image was generated using aerial photography taken in 1981.

are dominated by extensive outwash sheets of fluvial deposits and channel infill that represent the initial phase of erosion and sedimentation during the early glacial and inter-glacial periods. This was then followed by the advance of the Isere and surrounding glaciers and impounding of a lake, which was progressively infilled with varved glacio-lacustrine deposits. These deposits typically

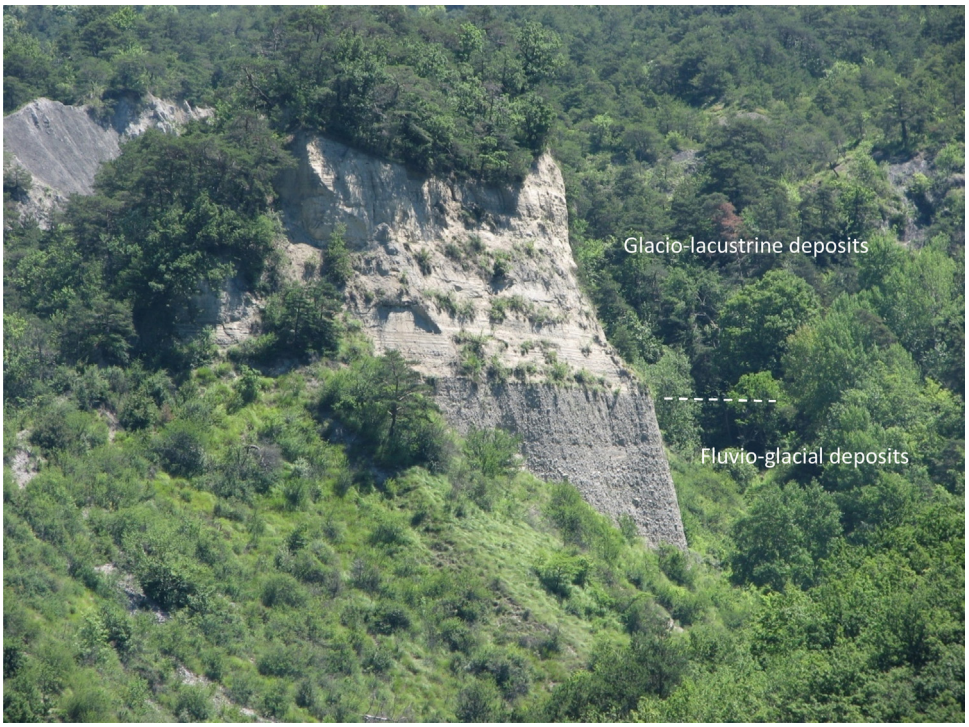

Fig. 4. Photograph showing the sharp contact between the basal coarse grained fluvio-glacial outwash deposits and the overlying glacial-lacustrine deposits, illustrating the dramatic and sudden drop in energy of the system from river to lake sediment deposition.

rest conformably on the fluvial deposits (Fig. 4) or in some places rest directly on the bedrock. The sharp contact between these two sequences (observed in Fig. 4) suggests a relatively sudden cessation of sediment input and switch to low energy glacio-lacustrine (lake) deposition. This was followed by a period during which the Isere Glacier fluctuated in extent, either retreating or advancing and over-riding the glacio-lacustrine deposits. This produced a series of basal till deposits that are interbedded with lacustrine deposits that reflect this period of ice fluctuation. With the end of this glaciation, ice retreat and the associated climatic amelioration, the river network gradually re-established within the valley, cutting through the Quaternary deposits to form the Drac river and the drainage network observed today. It is this sequence of events, the deposition of a thick sequence of Quaternary deposits and subsequent down cutting that has generated the conditions conducive to landsliding in this region.

Glacio-lacustrine deposits are very common in previously glaciated regions of the world, where pro-glacial lakes have formed in which thick sequences of laminated silts and clays (varves) have been deposited. Their geotechnical characteristics tend to lead to highly unstable behaviour (Fletcher et al., 2002), particularly where these deposits have been uplifted and subsequently eroded. Landslides in glacio-lacustrine deposits cause considerable ground related problems due to the highly sensitive nature of the geological materials, the retrogressive nature of the resulting large scale failures and the rapid conversion of this landslide material into mud flows once mobilised. The occurrence of landslides associated with glacio-lacustrine deposits have been well documented in the Alpine valleys of France (Jongmans et al., 2009), British Columbia in Canada (Evans, 1982; Jackson, 2002), Estonia and Baltic region (Kohv et al., 2010) and the Italian Alps (Tibaldi et al., 2004). In each case, the type of landsliding typically include rotational slides with mud flows developing in the displaced material and the evolution characteristics typically involve significant retrogressive behaviour (Geertsema et al., 2006; Marko et al., 2010). These landslides are often located in areas where varved clays are cut into by river erosion, reducing support and exposing bedding planes which dip down into the valleys (as a result of dip towards the centre of the previously ice-dammed lakes).

2. Data and methods

The aim of the project was to evaluate the use of image correlation techniques for landslide monitoring of the Harmaliere landslide using aerial photographic imagery. To this end, COSI-Corr image correlation software was used to process a sequence of aerial imagery and derive two sets of landslide displacement maps for the Hermaliere landslide. The data and methods are detailed as follows:

2.1. Image correlation techniques

Where two epochs of imagery are available for a landslide site, it is possible to compare these images manually using standard image interpretation to visually identify and map any changes that have occurred, and thereby identify areas of landslide movement. Digital image correlation, by contrast, uses statistical techniques to automatically match identical points in the two digital images and then measure their offset (in x and y) and by doing so, create a two dimensional displacement field across the landslide.

In this study, digital image correlation has been applied to a sequence of aerial photography using Cosi-Corr software (Ayoub et al., 2009; Leprince et al., 2007) in order to investigate the suitability of aerial imagery as the basis for landslide monitoring using image correlation. COSI-Corr applies Digital Image Correlation techniques using a normalised cross-correlation algorithm (NCC) to detect motions between two epochs of imagery (Leprince et al., 2007). It has been applied successfully in several types of surface movements such as earthquakes (Copley et al., 2011; Wei et al., 2011; Konca et al., 2010; Barisin et al., 2009; Barbot et al., 2008; Leprince et al., 2008, 2007; Taylor et al., 2008; Avouac et al., 2006), ice-flow (Heid and Kääb 2012; Debella-Gilo and Kaab 2011; Herman et al., 2011; Berthier et al., 2009; Quincey and Glasser 2009;

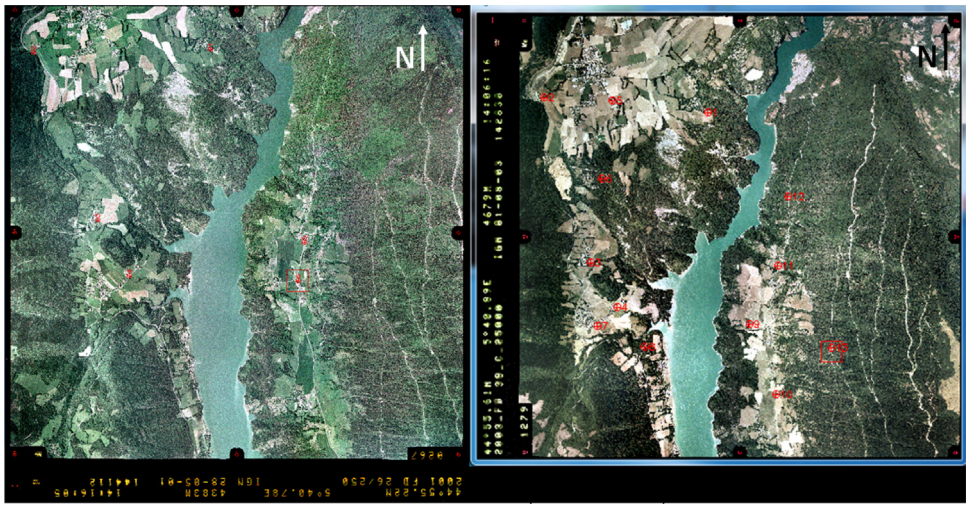

Fig. 5. GCPs distribution in 2001 photograph (left) as well as Tie points distribution over 2003 photograph (right).

Table 1
Characteristics of the image couplet used in the multi-temporal analysis.

Aerial images	Date	Scale	Flight direction	Time span (days)
2001_fd0026_250_c_0267	28/05/2001	1:23,733	S-N	783
2003_fd0038_250_c_1279	01/08/2003	1:25,830	W-E	

Tahayt et al., 2009; Leprince et al., 2008; Scherler et al., 2008), sand migrations (Hermas et al., 2012; Necsoiu et al., 2009; Vermeesch and Drake 2008) and landslide movement (Debella-Gilo and Kaab 2011; Leprince et al., 2008; Stumpf et al., 2014). These studies have typically used either high resolution satellite or topographic data but there have been few studies where aerial photography has been used as the basis for image correlation. In particular, landslide monitoring that has been undertaken using COSI-Corr have used satellite imagery rather than aerial photographs as is the case in this study.

2.2. Aerial imagery

The multi-temporal image correlation was performed using 1200 dpi digitalized aerial photographs purchased from the Institut Géographique National (IGN) for a three year period, from 2001 to 2003. Two sets of RGB (3 band images: Red (R), Green (G) and Blue (B)) colour aerial photographs for years 2001 and 2003 were chosen with similar altitudes, scale and illumination conditions. The flight scales were between 1:23,000 and 1:25,000 approximately and flight direction was either south to north and west to east (Table 1).

A combination of image pairs was chosen to minimise the temporal baselines between images in order to avoid potential decorrelation between image dates. However this technique does not require the use of image stereo pairs for each date, only a unique photograph that covers the entire area of interest is required. Therefore the photographs were chosen where the landslide was located in a more central position in the image (Table 1) (Fig. 4). However the stereoscopic effect could appear when we work with two images of the same area acquired from two different points of view, In order to minimise stereoscopic effects low and similar incidence angles, near to vertical incidence must be considered (Hermas et al., 2012; Van Puymbroeck et al., 2000). In Van Puymbroeck et al. (2000) they use the parameters of the images and a DEM to model and compensate the stereoscopic effect. In aerial photographs the geometry of the shot assures an almost vertical incidence angle that contributes to a negligible stereoscopic effect.

Camera calibration information was sourced for each of the image sets from the Institut Géographique National (IGN) and used alongside the aerial photography during the initial interior orientation stage.

2.3. Digital elevation model

The use of a digital elevation model is not mandatory when using COSI-Corr, however, in areas of high relief it is important incorporate an elevation model to correct for the topographic effects and distortions during the image matching process (Ayoub et al., 2009). In this study, we use the Advanced Spaceborne Thermal Emission and Reflection Radiometer (ASTER) Global Digital Elevation Model ASTER GDEM V2 at 30 m grid posting and acquired from USGS.

ASTER GDEM was released NASA and the Ministry of Economy, Trade and Industry (METI) of Japan as a contribution to the Global Earth Observing System of Systems (GEOSS). ASTER GDEM (GDEM1) was compiled from over 1.2 million scene-based DEMs covering land surfaces between 83°N and 83°Slatitudes. ASTER GDEM (GDEM2) was released by NASA and METI in mid-October, 2011 (Tachikawa et al., 2011). The GDEM2 has the same gridding and tile structure as GDEM1, but benefits from the inclusion of 260,000 additional scenes to improve coverage, a smaller correlation kernel (5×5 versus 9×9 for GDEM1) yielding higher spatial resolution, and improved water masking. The absolute vertical accuracy study found the GDEM2 to be within −0.20 m on average (ASTER GDEM V2 Validation Report, 2011).

2.4. Ground control points (GCPs)

GPS ground control data is required for image matching applied to aerial imagery in order to perform the exterior orientation of the photographs and orientate them with reference to the ground (Ayoub et al., 2009). In this study, the GPS ground control data were collected by researchers at the Université Joseph Fourier, Grenoble as part of a separate research project on the Harmaliere and Avignonet landslides (Bievre et al., 2011; Jongmans et al., 2009). The GPS data was collected during two different field campaigns and includes more than 40 ground control points (GCPs) distributed across the entire area outside the boundary of the active landslide. The entire area covers an extension bigger than the area recorded in a single image. For this reason some of the GCPs were not used

because they were outside the area recorded in the photographs used.

The campaigns were carried out with ASHTECH ProMark II devices with static acquisition method with 2 s measurement interval and 20 min observation time in each point. Resulting accuracy for these specifications and devices are establish in 5 mm + 1 ppm in horizontal and 10 mm + 2 ppm in vertical coordinates.

Fig. 5 shows the GCPs distribution in 2001 photograph (left) as well as Tie points distribution over 2003 photograph (right).

2.5. Workflow

The processing workflow for COSI-Corr is shown in Fig. 6 and comprises of five stages; interior and exterior orientation, *ortho*-rectification, resampling and final image correlation. The initial interior orientation establishes the relationship between the image and camera coordinate system using the fiducial marks on the image and the camera calibration report to provide a measure of the camera geometry and distortions (Wolf and Dewitt, 2000). Once complete, the imagery is further transformed during the exterior orientation, to real world coordinate space using GPS ground control points, that provide coordinate and height information for each point located in the imagery. Ayoub et al. (2009) recommend at least three ground control points per image for the exterior orientation, but in this study, we used a minimum of six points per photograph (Fig. 5). GCP were selected from the entire list of 40 points depending on if they were clearly identified in the images and their location to get a homogeneous distribution in each photograph. For the second Image 13 Tie points were selected by identifying homologous points manually in both images (2001 and 2003 photographs) to cover the entire frame surface (Fig. 5). The imagery was then *ortho*-rectified using the digital elevation model and known ground control points to remove terrain distortions and generate a geometrically accurate image that is then resampled to an agreed pixel size and coordinate system. Concretely in this study UTM coordinate system and bilinear resampling scheme were used.

When using colour aerial imagery with three RGB bands, then COSI-Corr will use only one of the bands for the re-sampling process. These steps follow the traditional photogrammetric workflow applied to aerial imagery (Wulf and Dewitt, 2000) but applied to one image and not the standard stereopair. Once the two sets of images have been generated for each data, COSI-Corr proceeds with the image correlation. COSI-Corr algorithms use a Normalized Cross-Correlation (NCC) to measure the similarity between matching entities in one image and their corresponding entity in a second image (Debella-Gilo and Kaab, 2011; Leprince et al., 2007). Once an object has been matched using its cross correlation, a Euclidean offset is computed between the two images to give a displacement in x and y. The resulting outputs include a West to East and North-South displacement field image and a vector displacement map.

For the correlation step, parameters must be defined and adapted manually during the processing. Given that the imagery used in this study can be considered noisy, Statistical Correlator Engine was selected in accordance with the Cosi_Corr userís guide recommendations (Ayoud et al., 2009).The parameters for this correlator include: window size in pixels, step in X and Y direction in pixels between two sliding windows and search range in X and Y direction in pixels for the displacements. In this study 10×10 pixels window size, 5 pixels step and 3 pixels search range in both X and Y directions were selected.

2.6. Accuracy assessment

According to Leprince et al. (2007) theoretical COSI-Corr subpixel accuracy is 1/50 pixel for satellite images with resolution no better than 5 m. It degrades at higher resolution (because of topographic roughness inducing more significant stereoscopic bias) of the order of 1/20th of the pixel size for aerial photographs with metric GSD (Ayoub et al., 2009). This value corresponds to 32.5 mm approximately in our research.

Given the activity of landslide, there are no monitoring points installed within the active parts of the slide, therefore accuracy assessment of the displacement field has been assessed using prior knowledge of the landslide movement (Stumpf et al., 2014), in our case, using field observations and airphoto interpretation.

3. Results

The results of the image matching between 2001 and 2003 are shown in Fig. 7. The figure shows the average movement direction derived from the north-south and east-west displacement fields. It presents areas with clear slope movement, areas of decorrelation or noise have been removed. The vector field shown in the figure is derived from the movement field generated from the image correlation and have been added manually to the figure to provide information on the movement direction and to improve clarity.

Zones of correlation indicate differing amounts of horizontal displacement of up to 2.5 m. There are three main zones of movement identified from the displacement field data. Firstly, a strong signature of landslide motion on the western flank of the landslide is detected. The differential settlement is well controlled by arcuate scarps defining a clear landslide zone in this portion of the landslide complex. Some regression is visible at the top of this slope with subsidence bounded by these scarps visible on the lower slopes. Localised de-correlation in this area can be related to the formation of a new mudflow in this area; and this event is visible in Fig. 7. The eastern flank also contains some displacement, particularly associated with several pre-existing lateral landslides that appear to be undergoing some deformation. The major displacement is associated with a second zone of decorrelation that again represents the signature of completely new landslides that have formed between the two image dates (2001–2003). Lastly, the head zone of the landslide contains more diffuse displacement data but within this zone, some major movement in the north-west section of landslide is observed moving down along the strike of the valley axis. There is evidence of some displacement in the north east portion of the head zone, particularly along the major scarp zone. Aerial photography does show some regression of this scarp between 2001 and 2003 and some major secondary movement just down slope. The apron of landslide debris within the centre of the Harmaliere valley identified by (Bievre et al., 2011) is clearly visible in the photography but shows no evidence of any major displacement. Indeed, much of the landslide movement is focused at the edges and back of the landslide and little movement is detected in the centre of the valley.

4. Discussion

The Harmaliere landslide has undergone major pulses of movement, starting in March 1981 with the first major advance followed by several major retrogressive events (Bievre et al., 2011). During the intervening period, the movement is characterised smaller scale flows and lateral movements. The short baseline used in this study has enabled this short temporal episodic movement to be imaged alongside the major movements between 2001 and 2003.

Bievre et al. (2011) mapped temporal landslide change across the Harmaliere landslide using aerial photographic interpretation for years 1956, 1985 and 2003. They used image thresholding to identify non-vegetated soils in the aerial photography and used this to identify areas of landslide activity. Their method appears to have overestimated the area of renewed activity, but despite this, for the epoch concurrent with our study (2003), they detect major

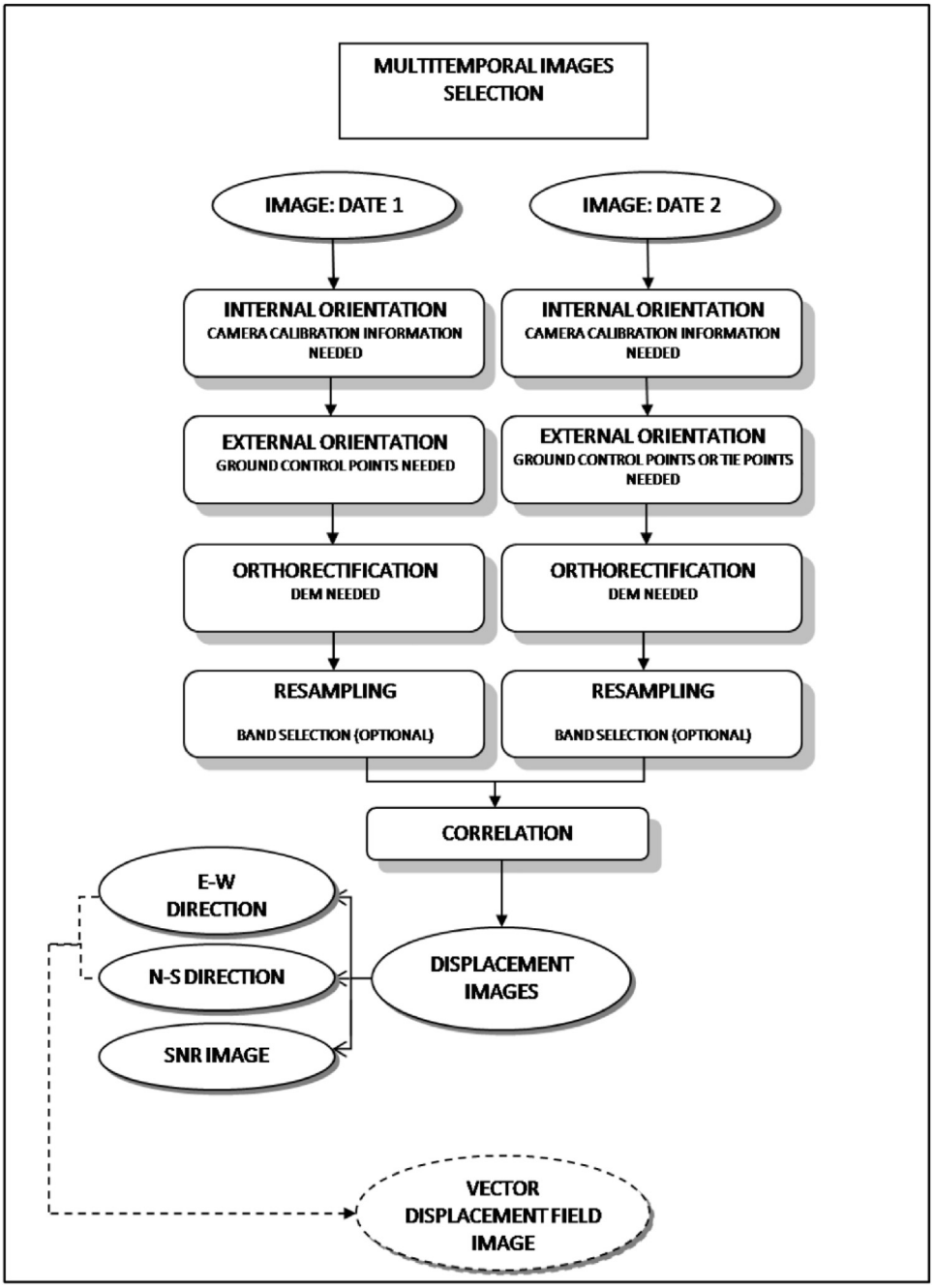

Fig. 6. Image matching workflow based upon aerial photographic imagery.

movement in the upper sections and west flanks of the landslide which are coincident with our results. However, the displacement data isolate a number of other areas of movement not identified in this previous study. Firstly, the eastern flank of the landslide is much more active, with at least three new landslides detected in the displacement data. Our results confirm that the western flank of the landslide in the lower part is undergoing significant movement, but highlights a second landslide with a similar movement rate, not previously observed. The displacement data indicates a strong component of movement for both these lateral landslides with displacements of up to 2.5 m for the period 2001–2003.

These results from our investigation suggest that the flanks of the Harmaliere landslide are undergoing some deformation and that this has important implications for future landslide behaviour. The lateral slope movements contribute significant material and debris into the main landslide in the Harmaliere valley. This is important when considering the geomorphological setting of the landslide; it is situated within a small catchment that funnels surface water down through the centre of the valley and into the main Drac valley. Surface runoff is therefore concentrated in the central axis of the Harmaliere valley and mobilises landslide debris that has accumulated at the bottom of the valley from these lateral landslide events. This helps to explain the flow style landslide behaviour that is observed in the lower part of the landslide system. The future behaviour of this lower part of the landslide may therefore be linked to the process of sediment input from lateral landslides, saturation and mobilisation of this debris, leading to reactivation of the lower portion of the landslide and ultimately the continued regression of the upper section and head of the landslide. Additionally, the head zone of the landslide is also affected by dis-

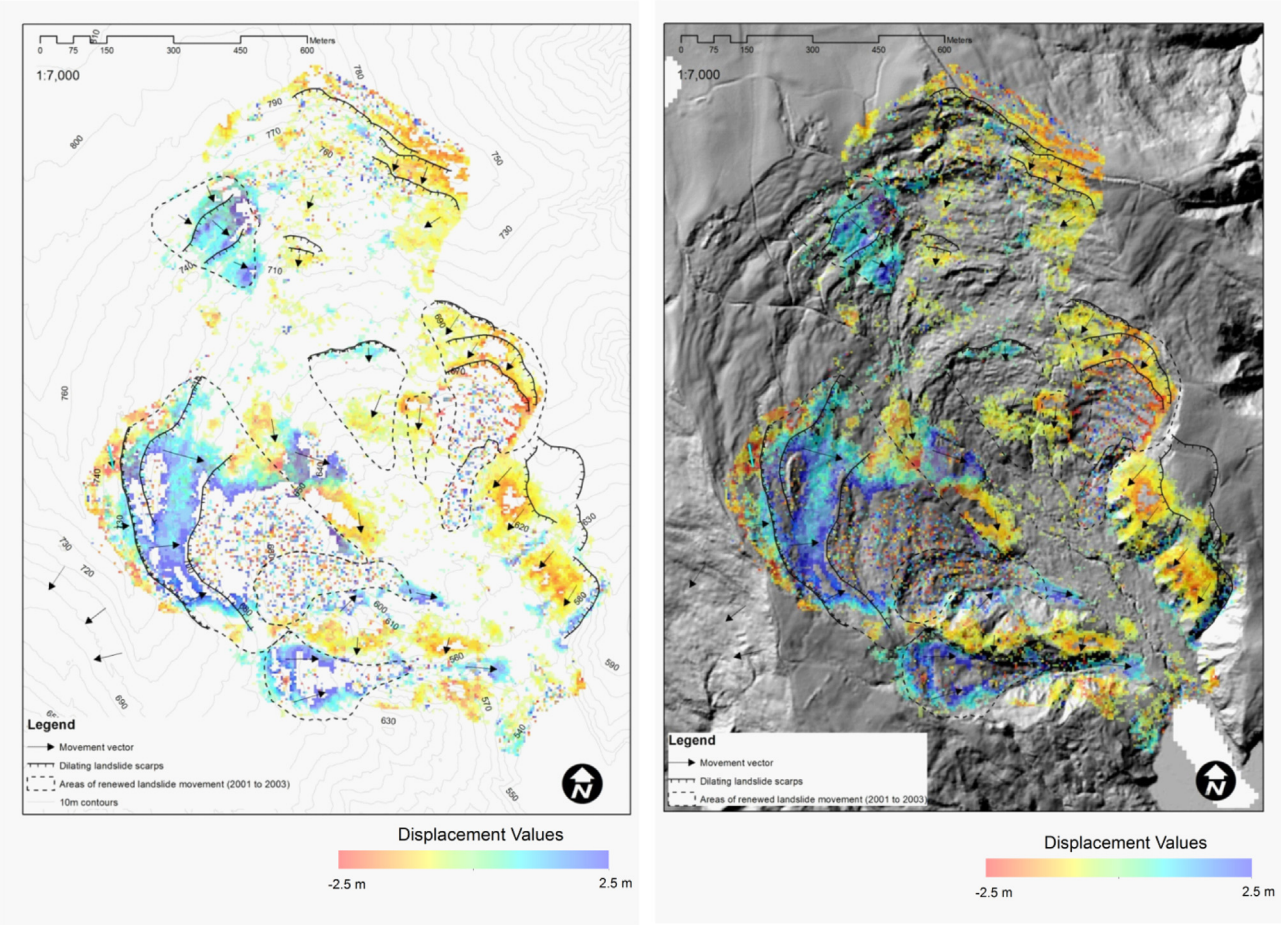

Fig. 7. Results of the image matching between 2001 and 2003 over contour lines (left) and DEM (right). Renewed landslide activity, scarps and slope movement vectors are shown. Displacement is cumulative over three years. Low SNR values have been mask to produce the image. Vector field displacement has been added as arrows movement direction over the image.

placement, particularly the eastern side of the scarp. This is also coincident with results from previous studies, which suggest that the axis of the Harmaliere landslide has shifted eastward and that this is an area of increased landslide movement (Bievre et al., 2011). Two major flank failures have been imaged in the displacement data. Two areas of de-correlation on the east and west flanks of the landslide can be observed in the displacement data and using image interpretation it is clear that these are associated with completely new landslide events (see Fig. 7). The de-correlation stems from the mis-match between the two images as a consequence of the appearance of new landslides that cannot be correlated between the images. Consequently, localised de-correlation should be not dismissed but, as in this case, may indicate the presence of new landslide activity.

Overall, the displacement data has helped us understand the behaviour of the landslide and identify particular areas of renewed activity. While we recognise that the rates of movement indicated by the displacement data for the period 2001–2003 cannot be validated (no GPS points are located in the Harmaliere valley), the overall motion of the landslide and areas of activity revealed by the image correlation are consistent with previous studies and qualitative observations from field reconnaissance and aerial photographic interpretation.

Within the measured zone, some regions are characterised by noise caused by decorrelation between the two images. These are caused by changes in surface cover, such as vegetation growth or areas of new slope movement that has occurred between the dates of the two images. The image analysis relies upon imagery that are free from shadow, snow and clouds so that the surface topography is fully visible in both images. In this study, images were taken in May 2001 and August 2003 respectively at 14:10 local time (Fig. 4) in order to minimise the presence of these limiting factors in the imagery.

5. Conclusions

This study has demonstrated the application of image cross-correlation to the study of landslide movement using aerial photographs for the first time. The analysis has provided important insights into the dynamics of the Harmaliere landslide between 2001 and 2003, and through this, we have been able to identify new movement and slope deformation not previously identified or quantified. The short temporal baseline has been shown to be not only a requirement for the successful implementation of COSI-Corr technique for landslide monitoring; but also an advantage, in allowing us to detect multi-temporal variations in the landslide movement that would have been invisible in longer baseline image sets.

Analysing landslide movement using aerial photography and image correlation techniques we have demonstrated that such monitoring is possible using aerial imagery, where high quality photography and ground control data are available. This new approach for landslide monitoring is likely to be of wide applicability to other areas characterised by complex ground displacements

where aerial photographs are available for a long temporal span. In this sense aerial photographs constitute an important source of information that could be use to this purpose not only by visual image interpretation but for automatic image correlation.

Acknowledgements

The authors are grateful to researchers at the Université Joseph Fourier, Grenoble for providing GPS control point data. The ASTER L1B data product was obtained through the online Data Pool at the NASA Land Processes Distributed Active Archive Center (LP DAAC), USGS/Earth Resources Observation and Science (EROS) Center, Sioux Falls, South Dakota (https://lpdaac.usgs.gov/data_access).

References

Antoine, D., 1992. CIPLAN: A Model-based System with Original Features for Understanding French plats. Centre de Recherche en Informatique.

ASTER Global Digital Elevtion Model Version 2–Summary of Validation Results. August31, 2011. http://www.jspacesystems.or.jp/ersdac/GDEM/ver2Validation/Summary_GDEM2_validation_report_final.pdf.

Avouac, J.P., Ayoub, F., Leprince, S., Konca, O., Helmberger, D., 2006. The 2005, Mw 7.6 Kashmir earthquake,rupture kinematics from sub-pixel correlation of ASTER images and seismic waveforms analysis. Earth Planet. Sci. Lett. 249 (3–4), 514–528.

Ayoub, F., Leprince, S., Avouac, J.P., 2009. Co-registration and correlation of aerial photographs for ground deformation measurements. Isprs J. Photogramm. Remote Sens. 64, 551–560.

Ayoud, F., Leprince, S., Keene, L., 2009. Userís Guide to COSI-CORR Co-Registration of Optically Sensed Images and Correlation. California .Institute of Technology http://www.tectonics.caltech.edu/slip_history/spot_coseis/pdf_files/cosi-corr_guide.pdf.

Barbot, S., Hamiel, Y., Fialko, Y., 2008. Space geodetic investigation of the coseismic and postseismic deformation due to the 2003 Mw7.2 Altai earthquake: implications for the local lithospheric rheology. J. Geophys. Res. 113, B03403, http://dx.doi.org/10.1029/2007JB005063.

Barisin, I., Leprince, S., Parsons, B., Wright, T., 2009. Surface displacements in the September 2005 Afar rifting event from satellite image matching: asymmetric uplift and faulting. Geophys. Res. Lett. 36, L07301, http://dx.doi.org/10.1029/2008GL036431.

Berthier, E., Le Bris, R., Mabileau, L., Testut, L., Rémy, F., 2009. Ice wastage on the kerguelen islands (49°S 69°E) between 1963 and 2006. J. Geophys. Res. 114, F03005, http://dx.doi.org/10.1029/2008JF001192.

Bievre, G., Kniess, U., Jongmans, D., Pathier, E., Schwartz, S., van Westen, C.J., Villemin, T., Zumbo, V., 2011. Paleotopographic control of landslides in lacustrine deposits (Trieves plateau French western Alps). Geomorphology 125, 214–224.

Booth, A.M., Lamb, M.P., Avouac, J.P., Delacourt, C., 2013. Landslide velocity, thickness, and rheology from remote sensing: la Clapière landslide, France. Geophys. Res. Lett. 40, 1–6, http://dx.doi.org/10.1002/grl.50828.

Casson, B., Delacourt, C., Baratoux, D., Allemand, P., 2003. Seventeen years of the "La Clapiere" landslide evolution analysed from ortho-rectified aerial photographs. Eng. Geol. 68, 123–139.

Copley, A., Avouac, J.P., Hollingsworth, J., Leprince, S., 2011. The 2001 M(w) 7.6 Bhuj earthquake, low fault friction, and the crustal support of plate driving forces in India. J. Geophys. Res. - Solid Earth 116, http://dx.doi.org/10.1029/2010jb008137 (article number: B08405).

Daehne, A., Corsini, A., 2013. Kinematics of active earthflows revealed by digital image correlation and DEM subtraction techniques applied to multi-temporal LiDAR data. Earth Surf. Processes Landforms 38, 640–654.

Debella-Gilo, M., Kaab, A., 2011. Sub-pixel precision image matching for measuring surface displacements on mass movements using normalized cross-correlation. Remote Sens. Environ. 115, 130–142.

Delacourt, C., Allemand, P., Berthier, E., Raucoules, D., Casson, B., Grandjean, P., Pambrun, C., Varel, E., 2007. Remote-sensing techniques for analysing landslide kinematics: a review. Bull. Soc. Geol. Fr. 178, 89–100.

Evans, S.G., 1982. Landslides and surficial deposits in urban areas of British Columbia: a review. Can. Geotech. J. 19, 269–288.

Fabris, M., Menin, A., Achilli, V., 2011. Landslide displacement estimation by archival digital photogrammetry. Ital. J. Remote Sens.-Riv. Ital. Telerilevamento 43, 23–30.

Fletcher, L., Hungr, O., Evans, S.G., 2002. Contrasting failure behaviour of two large landslides in clay and silt. Can. Geotech. J. 39, 46–62.

Gance, J., Malet, J.-P., Dewez, T., Travelletti, J., 2014. Target detection and tracking of moving objects for characterizing landslide displacements from time-lapse terrestrial optical images. Eng. Geol. 172, 26–40.

Geertsema, M., Clague, J.J., Schwab, J.W., Evans, S.G., 2006. An overview of recent large catastrophic landslides in northern British Columbia, Canada. Eng. Geol. 83 (1), 120–143.

Giraud, A., Antoine, P., Van Asch, T.W.J., Nieuwenhuis, J.D., 1991. Geotechnical problems caused by glaciolacustrine clays in the French Alps. Eng. Geol. 31, 185–195.

Heid, T., Kääb, A., 2012. Evaluation of existing image matching methods for deriving glacier surface displacements globally from optical satellite imagery. Remote Sens. Environ. 118, 339–355.

Herman, F., Anderson, B., Leprince, S., 2011. Mountain glacier velocity variation during a retreat advance cycle quantified using sub pixel analysis of ASTER images. J. Glaciol. 57 (202), 197–207.

Hermas, E., Leprince, S., El-Magd, I.A., 2012. Retrieving sand dune movements using sub-pixel correlation of multi-temporal optical remote sensing imagery, northwest Sinai Peninsula, Egypt. Remote Sens. Environ. 121, 51–60.

Jaboyedoff, M., Oppikofer, T., Abellán, A., Derron, M.H., Loye, A., Metzger, R., Pedrazzini, A., 2012. Use of LIDAR in landslide investigations: a review. Nat. Hazards 61 (1), 5–28.

Jackson, L.E., 2002. Landslides and landscape evolution in the Rocky Mountains and adjacent Foothills area, southwestern Alberta, Canada. Catastrophic Landslides: Effects Occurrence Mech. Geol. Soc. Am. Rev. Eng. Geol. 15, 325–344.

Jongmans, D., Renalier, F., Kniess, U., Schwartz, S., Pathier, E., Orengo, Y., Bievre, G., Villemin, T., Delacourt, C., 2008. Characterization of the Avignonet landslide (French Alps) with seismic techniques. Landslides Eng. Slopes: From Past Future 1 and 2, 395–401.

Jongmans, D., Bièvre, G., Renalier, F., Schwartz, S., Beaurez, N., Orengo, Y., 2009. Geophysical investigation of a large landslide in glaciolacustrine clays in the Trièves area (French Alps). Eng. Geol. 109, 45–56.

Kohv, M., Talviste, P., Hang, T., Kalm, V., 2010. Retrogressive slope failure in glaciolacustrine clays: sauga landslide, western Estonia. Geomorphology 124, 229–237.

Konca, A.O., Leprince, S., Avouac, J.P., Helmberger, D.V., 2010. Rupture process of the 1999 Mw 7. 1 Duzce earthquake from joint analysis of SPOT, GPS, InSAR, strong-motion, and teleseismic data: a supershear rupture with variable rupture velocity. Bull. Seismol. Soc. Am. 100 (1), 267–288, http://dx.doi.org/10.1785/0120090072.

Leprince, S., Barbot, S., Ayoub, F., Avouac, J.P., 2007. Automatic and precise orthorectification, coregistration, and subpixel correlation of satellite images, application to ground deformation measurements. Geosci. Remote Sens. IEEE Trans. 45, 1529–1558.

Leprince, S., Berthier, E., Ayoub, F., Delacourt, C., Avouac, J.P., 2008. Monitoring earth surface dynamics with optical imagery. EOS Trans. Am. Geophys. Union 89 (1), 1–2.

Marko, K., Tiit, H., Peeter, T., Volli, K., 2010. Analysis of a retrogressive landslide in glaciolacustrine varved clay. Eng. Geol. 116, 109–116.

Monserrat, O., Crosetto, M., Luzi, G., 2014. A review of ground-based SAR interferometry for deformation measurement. Isprs J. Photogramm. Remote Sens. 93, 40–48.

Necsoiu, M., Leprince, S., Hooper, D.M., Dinwiddie, C.L., McGinnis, R.N., Walter, G.R., 2009. Monitoring migration rates of an active subarctic dune field using optical imagery. Remote Sens. Environ. 113, 2441–2447.

Quincey, D.J., Glasser, N.F., 2007. Morphological and ice-dynamical changes on the tasman glacier, New Zealand, 1990–2007. Glob. Planet. Change 68 (3), 185–197.

Scherler, D., Bookhagen, B., Strecker, M.R., 2008. Spatially variable response of Himalayan glaciers to climate change affected by debris cover. Nat. Geosci., http://dx.doi.org/10.1038/ngeo1068 (23.01.08).

Stumpf, A., Malet, J.-P., Allemand, P., Ulrich, P., 2014. Surface reconstruction and landslide displacement measurements with Pléiades satellite images. Isprs J. Photogramm. Remote Sens. 95, 1–12.

Tachikawa, T., Hato, M., Kaku, M., Iwasaki, A., 2011. The Characteristics of ASTER GDEM version 2. IGARSS.

Tahayt, A., Feigl, K.L., Mourabit, T., Rigo, A., Reilinger, R., McClusky, S., Fadil, A., Berthier, E., Dorbath, L., Serroukh, M., Gomez, F., Ben Sari, D., 2009. The Al Hoceima (Morocco) earthquake of 24 February 2004, analysis and interpretation of data from ENVISAT ASAR and SPOT5 validated by ground-based observations. Remote Sens. Environ. 113 (2), 306–316, http://dx.doi.org/10.1016/j.rse.2008.09.015.

Taylor, M., Leprince, S., Avouac, J.P., Sieh, K., 2008. Detecting co-seismic displacements in glaciated regions: an example from the great november 2002 Denali earthquake using SPOT horizontal offsets. Earth Planet. Sci. Lett. 270 (3–4), 209–220.

Teza, G., Pesci, A., Genevois, R., Galgaro, A., 2008. Characterization of landslide ground surface kinematics from terrestrial laser scanning and strain field computation. Geomorphology 97, 424–437.

Tibaldi, A., Rovida, A., Corazzato, C., 2004. A giant deep-seated slope deformation in the Italian Alps studied by paleoseismological and morphometric techniques. Geomorphology 58, 27–47.

Travelletti, J., Delacourt, C., Allemand, P., Malet, J.P., Schmittbuhl, J., Toussaint, R., Bastard, M., 2012. Correlation of multi-temporal ground-based optical images for landslide monitoring: application, potential and limitations. Isprs J. Photogramm. Remote Sens. 70, 39–55.

Van Asch, T.W., Malet, J., Bogaard, T., 2009. The effect of groundwater fluctuations on the velocity pattern of slow-moving landslides. Nat. Hazards Earth Syst. Sci. 9, 739–749.

Van Puymbroeck, N., Michel, R., Binet, R., Avouac, J.P., Taboury, J., 2000. Measuring earthquakes from optical satellite images. Appl. Opt. 39 (20), 3486–3494.

Vermeesch, P., Drake, N., 2008. Remotely sensed dune celerity and sand flux measurements of the world's fastest barchans (Bodele, Chad). Geophys. Res. Lett. 35, L24404, http://dx.doi.org/10.1029/2008gl035921.
Wasowski, J., Bovenga, F., 2014. Investigating landslides and unstable slopes with satellite multi temporal interferometry: current issues and future perspectives. Eng. Geol. 174, 103–138.
Wei, S., Fielding, E., Leprince, S., Sladen, A., Avouac, J.P., Helmberger, D., Hauksson, E., Chu, R., Simons, M., Hudnut, K., Herring, T., Briggs, R., 2011. Superficial simplicity of the 2010 El mayor-Cucapah earthquake of baja california in Mexico. Nat. Geosci. 4 (9), 615–618, http://dx.doi.org/10.1038/ngeo1213.
Wolf, P.R., Dewitt, B.A., 2000. Elements of Photogrammetry, Third Edition. McGraw-Hill, Boston.